

## Fabrication of $\text{NaLa}(\text{MoO}_4)_2 : \text{Ho}^{3+}/\text{Yb}^{3+}/\text{Tm}^{3+}$ White Phosphors via MSG Process and Their UC Photoluminescence Properties

Won-Chun Oh, Ji Soon Park, Eung Gyun Kim, Hak Su Kim and  
Chang Sung Lim\*

Department of Aerospace Advanced Materials & Chemical Engineering, Hanseo University,  
Seosan 356-706, Korea

---

**Abstract:** White phosphors of  $\text{NaLa}_{1-x}(\text{MoO}_4)_2$  doped with  $\text{Yb}^{3+}$  for a sensitizer and  $\text{Ho}^{3+}/\text{Tm}^{3+}$  for activators were successfully fabricated, and their upconversion(UC) properties were investigated. The resultant particles showed up well-crystallized and homogeneous morphologies with 3-5  $\mu\text{m}$  of particle sizes. Under excitation derived from 980 nm, the final particles led to the formation of white emissions composed of the red, green, and blue emission features, which are resulted from the transitions of  $\text{Tm}^{3+}$  from the  ${}^1\text{G}_4 \rightarrow {}^3\text{H}_6$  in the blue emission area, the transitions of  $\text{Ho}^{3+}$  from the  ${}^5\text{S}_2/{}^5\text{F}_4 \rightarrow {}^5\text{I}_8$  in the green emission area, as well as the transitions of  $\text{Ho}^{3+}$  from the  ${}^5\text{F}_5 \rightarrow {}^5\text{I}_8$  and the transitions of  $\text{Tm}^{3+}$  from the  ${}^1\text{G}_4 \rightarrow {}^3\text{F}_4$  and  ${}^3\text{H}_4 \rightarrow {}^3\text{H}_6$  in the red emission area. The dependence for pump power, chromaticity coordinates of CIE, and Raman spectroscopic feature of the synthesized phosphors were discussed in detail.

**Key words:** White emission,  $\text{Ho}^{3+}/\text{Yb}^{3+}/\text{Tm}^{3+}$  tri-doped,  $\text{NaLa}(\text{MoO}_4)_2$  phosphors, Upconversion properties

---

### Introduction

Recently, rare-earth doped upconversion (UC) particles can convert near infrared radiation of low energy into visible radiation of high energy. The synthesis and the luminescence properties of UC particles have evolved in their applications, since they are considered as potentially active components in new optoelectronic devices and luminescent labels for imaging and biodetection assays, which overcome the current limitations in traditional photoluminescence materials [1-3]. Double molybdates  $\text{NaLn}(\text{MoO}_4)_2$  ( $\text{Ln} = \text{La}^{3+}, \text{Y}^{3+}$  and  $\text{Gd}^{3+}$ ) compounds belong to the space group  $I4_1/a$  with the tetragonal phase, and have the family of sheelite-type structure [4, 5]. The trivalent lanthanide ions are partially substituted into the crystalline lattices of the tetragonal double tungstate crystal phase. The possible doping could be attributed to the very similar radii of the trivalent lanthanide ions and bring excellent properties for UC photoluminescence [6]. White emissions can be generated

---

\* Corresponding author: [cslim@hanseo.ac.kr](mailto:cslim@hanseo.ac.kr)

via a tri-doping system based on the blue, green, and red emission bands. Many lanthanide doping materials, such as laser active  $\text{Ho}^{3+}$  and  $\text{Tm}^{3+}$ , are employed as an activator in luminescent centers for  $\text{Yb}^{3+}$  as a sensitizer, because of their unique electronic energy levels. The tri-doped  $\text{Yb}^{3+}$ ,  $\text{Ho}^{3+}$ , and  $\text{Tm}^{3+}$  ions can remarkably enhance the UC efficiency for the shift from infrared to visible light because of the efficiency of the energy transfer from  $\text{Yb}^{3+}$  to  $\text{Ho}^{3+}$  and  $\text{Yb}^{3+}$  to  $\text{Tm}^{3+}$ .  $\text{Ho}^{3+}$  exhibits  $^5\text{S}_2/ ^5\text{F}_4 \rightarrow ^5\text{I}_8$  transitions in the green region,  $^5\text{F}_5 \rightarrow ^5\text{I}_8$  transitions in the red region in the UC process, and  $\text{Tm}^{3+}$  shows the  $^1\text{G}_4 \rightarrow ^3\text{H}_6$  transitions in the blue region, and  $^1\text{G}_4 \rightarrow ^3\text{F}_4$  and  $^3\text{H}_4 \rightarrow ^3\text{H}_6$  transitions in the red region [7-9]. These ions are effectively doped into the crystal lattices of the tetragonal phase because of the similar radii of the trivalent rare-earth ions; this results in high red-emitting efficiency, and superior thermal and chemical stability in the white emitting diode.

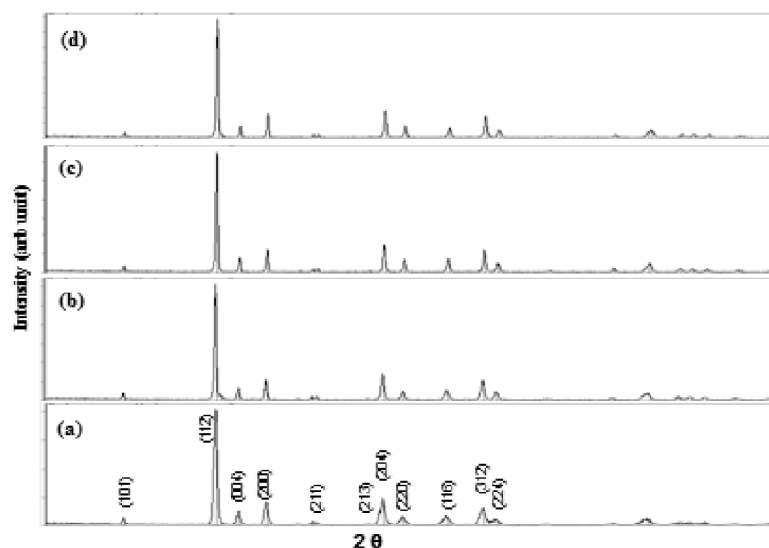
For fabrication of the double molybdate  $\text{NaLn}(\text{MoO}_4)_2$ , several specific processes have been developed, including solid-state reactions [10-13], the sol-gel method [14, 15], the Czochralski method [16-19], the hydrothermal method [20-24], the microwave assisted hydrothermal method [25], and pulse laser deposition [26]. Compared to the usual methods, microwave synthesis has the advantages of a very short reaction time, small-size particles, narrow particle-size distribution, and high purity of the final polycrystalline samples [27]. However, the fabrication of  $\text{Ho}^{3+}/\text{Yb}^{3+}/\text{Tm}^{3+}$  tri-doped  $\text{NaLa}(\text{MoO}_4)_2$  phosphors via the microwave sol-gel (MSG) process has not been reported. In this study, the double molybdate  $\text{NaGd}(\text{MoO}_4)_2$  phosphors with the proper doping concentrations of  $\text{Ho}^{3+}$ ,  $\text{Yb}^{3+}$  and  $\text{Tm}^{3+}$  ( $x = \text{Ho}^{3+} + \text{Yb}^{3+} + \text{Tm}^{3+}$ ,  $\text{Ho}^{3+} = 0.04, 0.03, 0.02, 0.01$ ,  $\text{Yb}^{3+} = 0.35, 0.40, 0.45, 0.50$  and  $\text{Tm}^{3+} = 0.01, 0.02, 0.03, 0.04$ ) were successfully prepared by the MSG process, followed by heat treatment. The synthesized particles were characterized by X-ray diffraction (XRD) and scanning electron microscopy (SEM). The pump power dependence of the UC emission intensity and Commission Internationale de L'Eclairage (CIE) chromatic coordinates were evaluated in detail. The optical properties were examined comparatively using photoluminescence (PL) emission and Raman spectroscopy.

## Experimental

Appropriate stoichiometric amounts of  $\text{Na}_2\text{MoO}_4 \cdot 2\text{H}_2\text{O}$  (99%, Sigma-Aldrich, USA),  $\text{La}(\text{NO}_3)_3 \cdot 6\text{H}_2\text{O}$  (99%, Sigma-Aldrich, USA),  $(\text{NH}_4)_6\text{Mo}_7\text{O}_{24} \cdot 4\text{H}_2\text{O}$  (99%, Alfa Aesar, USA),  $\text{Ho}(\text{NO}_3)_3 \cdot 5\text{H}_2\text{O}$  (99.9%, Sigma-Aldrich, USA),  $\text{Yb}(\text{NO}_3)_3 \cdot 5\text{H}_2\text{O}$  (99.9%, Sigma-Aldrich, USA),  $\text{Tm}(\text{NO}_3)_3 \cdot 5\text{H}_2\text{O}$  (99.9%, Sigma-Aldrich, USA), citric acid (99.5%, Daejung Chemicals, Korea),  $\text{NH}_4\text{OH}$  (A.R.), ethylene glycol (A.R.), and distilled water were used to prepare the compounds. To prepare  $\text{NaLa}_{0.60}(\text{MoO}_4)_2 \cdot \text{Ho}_{0.04}/\text{Yb}_{0.35}/\text{Tm}_{0.01}$ , 0.2 mol%  $\text{Na}_2\text{MoO}_4 \cdot 2\text{H}_2\text{O}$  and 0.114 mol%  $(\text{NH}_4)_6\text{Mo}_7\text{O}_{24} \cdot 4\text{H}_2\text{O}$  were dissolved in 20 mL of ethylene glycol and 80 mL of 5M  $\text{NH}_4\text{OH}$  under vigorous stirring and heating. Subsequently, 0.24 mol%  $\text{La}(\text{NO}_3)_3 \cdot 6\text{H}_2\text{O}$  with 0.016 mol%  $\text{Ho}(\text{NO}_3)_3 \cdot 5\text{H}_2\text{O}$ , 0.14 mol%  $\text{Yb}(\text{NO}_3)_3 \cdot 5\text{H}_2\text{O}$ , 0.004 mol%  $\text{Tm}(\text{NO}_3)_3 \cdot 5\text{H}_2\text{O}$ , and citric acid (with a molar ratio of citric acid to total metal ions of 2:1) were dissolved in 100 mL of distilled water under vigorous stirring and heating. Then, the solutions were mixed together under vigorous stirring and heating at 80 to 100°C. Finally, highly transparent solutions were obtained and adjusted to  $\text{pH} = 7-8$  by the addition

of 8M  $\text{NH}_4\text{OH}$ . In order to prepare  $\text{NaLa}_{0.55}(\text{MoO}_4)_2:\text{Ho}_{0.03}/\text{Yb}_{0.40}/\text{Tm}_{0.02}$ , the mixture of 0.22 mol%  $\text{La}(\text{NO}_3)_3 \cdot 6\text{H}_2\text{O}$  with 0.012 mol%  $\text{Ho}(\text{NO}_3)_3 \cdot 5\text{H}_2\text{O}$ , 0.16 mol%  $\text{Yb}(\text{NO}_3)_3 \cdot 5\text{H}_2\text{O}$ , and 0.008 mol%  $\text{Tm}(\text{NO}_3)_3 \cdot 5\text{H}_2\text{O}$  was used to create the rare-earth solution. In order to prepare  $\text{NaLa}_{0.50}(\text{MoO}_4)_2:\text{Ho}_{0.02}/\text{Yb}_{0.45}/\text{Tm}_{0.03}$ , the mixture of 0.20 mol%  $\text{La}(\text{NO}_3)_3 \cdot 6\text{H}_2\text{O}$  with 0.008 mol%  $\text{Ho}(\text{NO}_3)_3 \cdot 5\text{H}_2\text{O}$ , 0.18 mol%  $\text{Yb}(\text{NO}_3)_3 \cdot 5\text{H}_2\text{O}$ , and 0.012 mol%  $\text{Tm}(\text{NO}_3)_3 \cdot 5\text{H}_2\text{O}$  was used to create the rare-earth solution. In order to prepare  $\text{NaLa}_{0.45}(\text{MoO}_4)_2:\text{Ho}_{0.01}/\text{Yb}_{0.50}/\text{Tm}_{0.04}$ , the rare-earth containing solution was generated using 0.18 mol%  $\text{La}(\text{NO}_3)_3 \cdot 6\text{H}_2\text{O}$  with 0.004 mol%  $\text{Ho}(\text{NO}_3)_3 \cdot 5\text{H}_2\text{O}$ , 0.20 mol%  $\text{Yb}(\text{NO}_3)_3 \cdot 5\text{H}_2\text{O}$ , and 0.016 mol%  $\text{Tm}(\text{NO}_3)_3 \cdot 5\text{H}_2\text{O}$ .

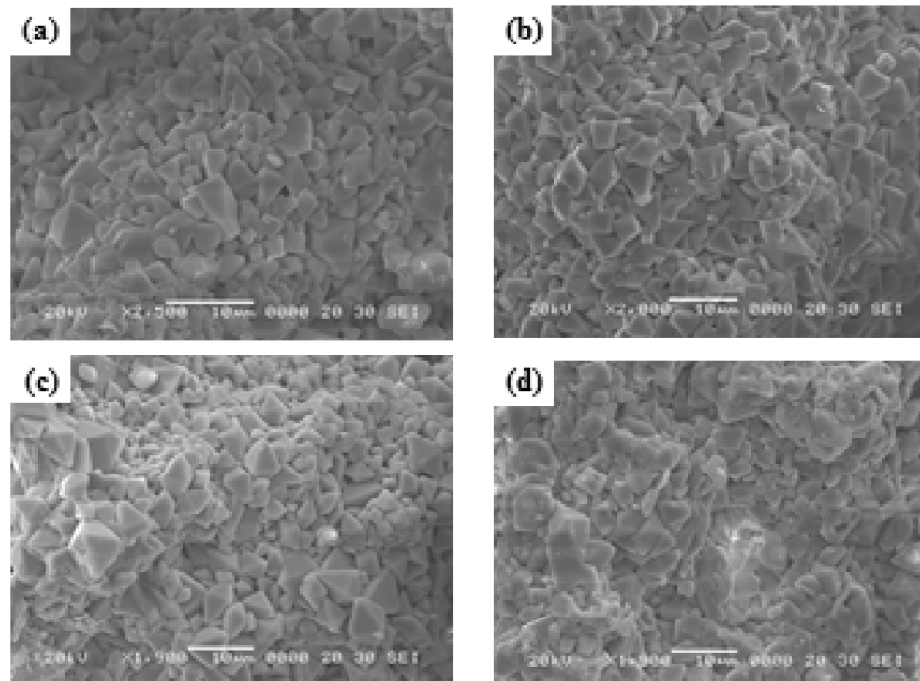
The transparent solutions were placed in a microwave oven operating at a frequency of 2.45 GHz with a maximum output power of 1250 W for 30 min. The working cycle of the microwave reaction was controlled very precisely using a regime of 40 s on and 20 s off for 15 min, followed by further treatment of 30 s on and 30 s off for 15 min. The samples were treated with ultrasonic radiation for 10 min to produce a light-yellow transparent sol. After this, the light-yellow transparent sols were dried at  $120^\circ\text{C}$  in a dry oven to obtain black dried gels, which were ground and heat-treated at  $800^\circ\text{C}$  for 16 h with  $100^\circ\text{C}$  intervals between 600 and  $800^\circ\text{C}$ . Finally, pink particles were obtained for the doped compositions. The phase composition of the synthesized particles was identified using XRD (D/MAX 2200, Rigaku, Japan). The microstructure and surface morphology of the synthesized particles were observed using SEM (JSM-5600, JEOL, Japan). The PL spectra were recorded using a spectrophotometer (Perkin Elmer LS55, UK) at room temperature. Raman spectroscopy measurements were performed using a LabRam Aramis (Horiba Jobin-Yvon, France). The 514.5-nm line of an Ar ion laser was used as the excitation source, and the power on the samples was kept at 0.5 mW.



**Figure 1:** X-ray diffraction patterns of the (a)  $\text{NaLa}_{0.60}(\text{MoO}_4)_2:\text{Ho}_{0.04}/\text{Yb}_{0.35}/\text{Tm}_{0.01}$ , (b)  $\text{NaLa}_{0.55}(\text{MoO}_4)_2:\text{Ho}_{0.03}/\text{Yb}_{0.40}/\text{Tm}_{0.02}$ , (c)  $\text{NaLa}_{0.50}(\text{MoO}_4)_2:\text{Ho}_{0.02}/\text{Yb}_{0.45}/\text{Tm}_{0.03}$ , and (d)  $\text{NaLa}_{0.45}(\text{MoO}_4)_2:\text{Ho}_{0.01}/\text{Yb}_{0.50}/\text{Tm}_{0.04}$  particles.

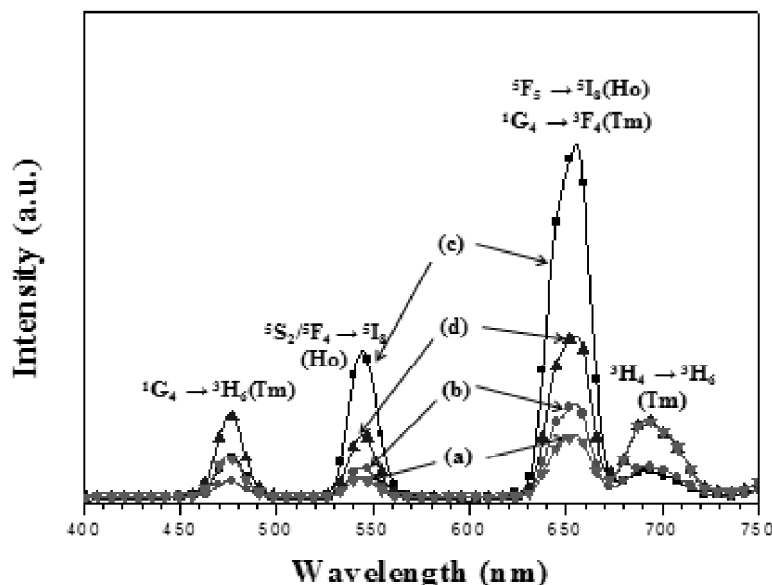
## Results and Discussion

Fig. 1 shows the X-ray diffraction patterns of the synthesized (a)  $\text{NaLa}_{0.60}(\text{MoO}_4)_2:\text{Ho}_{0.04}/\text{Yb}_{0.35}/\text{Tm}_{0.01}$ , (b)  $\text{NaLa}_{0.55}(\text{MoO}_4)_2:\text{Ho}_{0.03}/\text{Yb}_{0.40}/\text{Tm}_{0.02}$ , (c)  $\text{NaLa}_{0.50}(\text{MoO}_4)_2:\text{Ho}_{0.02}/\text{Yb}_{0.45}/\text{Tm}_{0.03}$ , and (d)  $\text{NaLa}_{0.45}(\text{MoO}_4)_2:\text{Ho}_{0.01}/\text{Yb}_{0.50}/\text{Tm}_{0.04}$  particles. All the XRD peaks could be assigned to the tetragonal-phase  $\text{NaLa}(\text{MoO}_4)_2$  with the space group of  $I4_1/a$ , which was in good agreement with the crystallographic data of  $\text{NaLa}(\text{MoO}_4)_2$  (JCPDS 25-0828).  $\text{NaLa}(\text{MoO}_4)_2$  as a member of double molybdate family has a sheelite structure with the lattice constants of  $a=5.344 \text{ \AA}$  and  $c=11.730 \text{ \AA}$  [19]. In pure  $\text{NaLa}(\text{MoO}_4)_2$  crystals, the unit cell decrease occurs because of the substitution of  $\text{Ho}^{3+}$  ( $R = 1.015 \text{ \AA}$ ),  $\text{Yb}^{3+}$  ( $R = 0.985 \text{ \AA}$ ) and  $\text{Tm}^{3+}$  ( $R = 0.994 \text{ \AA}$ ) ions in the  $\text{La}^{3+}$  ( $R=0.16 \text{ \AA}$ ) sites [28]. Post heat-treatment plays an important role in a well-defined crystallized morphology. To achieve a well-defined crystalline morphology of  $\text{NaLa}_{0.60}(\text{MoO}_4)_2:\text{Ho}_{0.04}/\text{Yb}_{0.35}/\text{Tm}_{0.01}$ ,  $\text{NaLa}_{0.55}(\text{MoO}_4)_2:\text{Ho}_{0.03}/\text{Yb}_{0.40}/\text{Tm}_{0.02}$ ,  $\text{NaLa}_{0.50}(\text{MoO}_4)_2:\text{Ho}_{0.02}/\text{Yb}_{0.45}/\text{Tm}_{0.03}$  and  $\text{NaLa}_{0.45}(\text{MoO}_4)_2:\text{Ho}_{0.01}/\text{Yb}_{0.50}/\text{Tm}_{0.04}$  particles, phases need to be heat treated at  $800^\circ\text{C}$  for 16 h. It is assumed that the doping amount of  $\text{Ho}^{3+}/\text{Yb}^{3+}/\text{Tm}^{3+}$  has a great effect on the crystalline cell volume of the  $\text{NaLa}(\text{MoO}_4)_2$ , because of the different ionic sizes. That is, the obtained samples possess a tetragonal phase after partial substitution of  $\text{La}^{3+}$  by  $\text{Ho}^{3+}$ ,  $\text{Yb}^{3+}$ , and  $\text{Tm}^{3+}$  ions, which are effectively doped into the crystal lattices of the  $\text{NaLa}(\text{MoO}_4)_2$  phase because of the similar radii of  $\text{La}^{3+}$ ,  $\text{Ho}^{3+}$ ,  $\text{Yb}^{3+}$ , and  $\text{Tm}^{3+}$ .



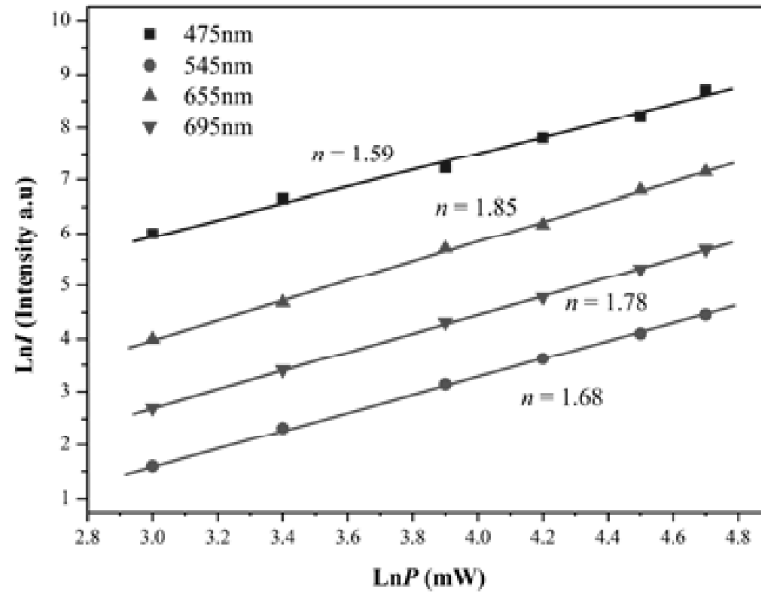
**Figure 2:** Scanning electron microscopy images of the synthesized (a)  $\text{NaLa}_{0.60}(\text{MoO}_4)_2:\text{Ho}_{0.04}/\text{Yb}_{0.35}/\text{Tm}_{0.01}$ , (b)  $\text{NaLa}_{0.55}(\text{MoO}_4)_2:\text{Ho}_{0.03}/\text{Yb}_{0.40}/\text{Tm}_{0.02}$ , (c)  $\text{NaLa}_{0.50}(\text{MoO}_4)_2:\text{Ho}_{0.02}/\text{Yb}_{0.45}/\text{Tm}_{0.03}$ , and (d)  $\text{NaLa}_{0.45}(\text{MoO}_4)_2:\text{Ho}_{0.01}/\text{Yb}_{0.50}/\text{Tm}_{0.04}$  particles.

Fig. 2 shows SEM images of the synthesized (a)  $\text{NaLa}_{0.60}(\text{MoO}_4)_2:\text{Ho}_{0.04}/\text{Yb}_{0.35}/\text{Tm}_{0.01}$ , (b)  $\text{NaLa}_{0.55}(\text{MoO}_4)_2:\text{Ho}_{0.03}/\text{Yb}_{0.40}/\text{Tm}_{0.02}$ , (c)  $\text{NaLa}_{0.50}(\text{MoO}_4)_2:\text{Ho}_{0.02}/\text{Yb}_{0.45}/\text{Tm}_{0.03}$ , and (d)  $\text{NaLa}_{0.45}(\text{MoO}_4)_2:\text{Ho}_{0.01}/\text{Yb}_{0.50}/\text{Tm}_{0.04}$  particles. The as-synthesized samples have similar morphologies and no discrepancy in morphological features, showing well crystallized and homogeneous microcrystalline morphology with a particle size of 3–5  $\mu\text{m}$ . In particular, the strongly agglomerated morphology of the particles can be observed by the atom inter-diffusion between the grains. The MSG process in application to the double molybdates provides the energy to synthesize the bulk of the material uniformly, so that fine particles with controlled morphology can be fabricated in a short time. The method is a cost-effective way to fabricate highly homogeneous products with easy scale-up. It is a viable alternative for the rapid synthesis of UC particles. This suggests that the MSG route is suitable for the creation of homogeneous  $\text{NaLa}_{1-x}(\text{MoO}_4)_2:\text{Ho}^{3+}/\text{Yb}^{3+}/\text{Tm}^{3+}$  crystallites.



**Figure 3:** Upconversion photoluminescent emission spectra of (a)  $\text{NaLa}_{0.60}(\text{MoO}_4)_2:\text{Ho}_{0.04}/\text{Yb}_{0.35}/\text{Tm}_{0.01}$ , (b)  $\text{NaLa}_{0.55}(\text{MoO}_4)_2:\text{Ho}_{0.03}/\text{Yb}_{0.40}/\text{Tm}_{0.02}$ , (c)  $\text{NaLa}_{0.50}(\text{MoO}_4)_2:\text{Ho}_{0.02}/\text{Yb}_{0.45}/\text{Tm}_{0.03}$ , and (d)  $\text{NaLa}_{0.45}(\text{MoO}_4)_2:\text{Ho}_{0.01}/\text{Yb}_{0.50}/\text{Tm}_{0.04}$  particles excited under 980 nm at room temperature.

Fig. 3 shows the UC photoluminescence emission spectra of the as-prepared (a)  $\text{NaLa}_{0.60}(\text{MoO}_4)_2:\text{Ho}_{0.04}/\text{Yb}_{0.35}/\text{Tm}_{0.01}$ , (b)  $\text{NaLa}_{0.55}(\text{MoO}_4)_2:\text{Ho}_{0.03}/\text{Yb}_{0.40}/\text{Tm}_{0.02}$ , (c)  $\text{NaLa}_{0.50}(\text{MoO}_4)_2:\text{Ho}_{0.02}/\text{Yb}_{0.45}/\text{Tm}_{0.03}$ , and (d)  $\text{NaLa}_{0.45}(\text{MoO}_4)_2:\text{Ho}_{0.01}/\text{Yb}_{0.50}/\text{Tm}_{0.04}$  particles. Under excitation at 980 nm at room temperature, the doped particles exhibited white emissions based on blue, green, and red emission bands, which correspond to the  $^1\text{G}_4 \rightarrow ^3\text{H}_6$  transitions of  $\text{Tm}^{3+}$  in the blue region, the  $^5\text{S}_2/\text{}^5\text{F}_4 \rightarrow ^5\text{I}_8$  transitions of  $\text{Ho}^{3+}$  in the green region, and the  $^5\text{F}_5 \rightarrow ^5\text{I}_8$  transitions of  $\text{Ho}^{3+}$ , as well as the  $^1\text{G}_4 \rightarrow ^3\text{F}_4$  and  $^3\text{H}_4 \rightarrow ^3\text{H}_6$  transitions of  $\text{Tm}^{3+}$ , in the red region. The UC intensity of (c)  $\text{NaLa}_{0.50}(\text{MoO}_4)_2:\text{Ho}_{0.02}/\text{Yb}_{0.45}/\text{Tm}_{0.03}$  provides the strongest 545-nm emission band in the green region, and the strongest 655-



**Figure 4:** Logarithmic scale dependence of the upconversion emission intensity on the pump power in the range from 20 to 110 mW at 475, 545, 655, and 695 nm in the  $\text{NaLa}_{0.50}(\text{MoO}_4)_2:\text{Ho}_{0.02}/\text{Yb}_{0.45}/\text{Tm}_{0.03}$  sample.

nm emission band in the red region because of the appropriate ratio of  $\text{Yb}^{3+}:\text{Ho}^{3+}+\text{Tm}^{3+} = 9:1$ . Thus, the optimal  $\text{Yb}^{3+}:\text{Ho}^{3+}+\text{Tm}^{3+}$  ratio is as high as 9:1 for the white emitting diode based on the blue, green, and red emissions.

The logarithmic scale dependence of the UC emission intensities at 475, 545, 655, and 695 nm on the working pump power over the range of 20 to 110 mW in the  $\text{NaLa}_{0.50}(\text{MoO}_4)_2:\text{Yb}_{0.02}/\text{Ho}_{0.45}/\text{Tm}_{0.03}$  sample is shown in Fig. 4. In the UC process, the UC emission intensity is proportional to the slope value  $n$  of the irradiation pumping power, where  $n$  is the number of pumped photons required to produce UC emission [29]:

$$I \propto P^n \quad (1)$$

$$\text{Ln}I \propto n\text{Ln}P \quad (2)$$

where  $I$  is the UC luminescent intensity, and  $P$  is the laser pumping power. As is evident from Fig. 4, the slope value calculations indicate  $n = 1.59$  for green emission at 475 nm,  $n = 1.68$  for green emission at 545 nm, and  $n = 1.85$  and  $1.78$  for red emissions at 655 and 695 nm, respectively.

Fig. 5 shows (A) calculated chromaticity coordinates ( $x$ ,  $y$ ) values and (B) CIE chromaticity diagram for (a)  $\text{NaLa}_{0.60}(\text{MoO}_4)_2:\text{Ho}_{0.04}/\text{Yb}_{0.35}/\text{Tm}_{0.01}$ , (b)  $\text{NaLa}_{0.55}(\text{MoO}_4)_2:\text{Ho}_{0.03}/\text{Yb}_{0.40}/\text{Tm}_{0.02}$ , (c)  $\text{NaLa}_{0.50}(\text{MoO}_4)_2:\text{Ho}_{0.02}/\text{Yb}_{0.45}/\text{Tm}_{0.03}$ , and (d)  $\text{NaLa}_{0.45}(\text{MoO}_4)_2:\text{Ho}_{0.01}/\text{Yb}_{0.50}/\text{Tm}_{0.04}$  particles. In Fig. 6 (A) the calculated chromaticity coordinates ( $x$ ,  $y$ ) and (B) CIE chromaticity diagrams are shown for the compositions (a)-(d). The triangle in Fig. 6(B) indicates standard coordinates for blue, green, and red. The inset in Fig. 6(B)

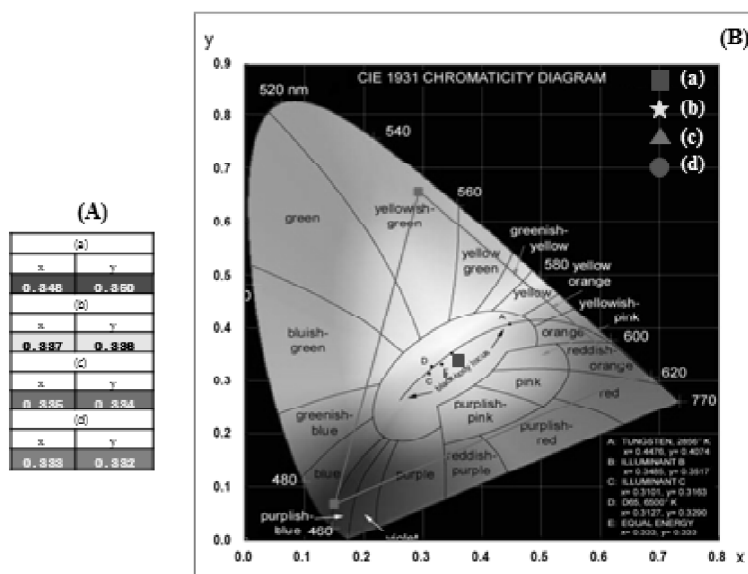


**Figure 5:** (A) Calculated chromaticity coordinates ( $x, y$ ) values and (B) CIE chromaticity diagram for  $\text{NaLa}_x(\text{MoO}_4)_2:\text{Ho}^{3+}/\text{Yb}^{3+}/\text{Tm}^{3+}$  phosphors. The inset shows the emission points for the sample synthesized (a)  $\text{NaLa}_{0.60}(\text{MoO}_4)_2:\text{Ho}_{0.04}/\text{Yb}_{0.35}/\text{Tm}_{0.01}$ , (b)  $\text{NaLa}_{0.55}(\text{MoO}_4)_2:\text{Ho}_{0.03}/\text{Yb}_{0.40}/\text{Tm}_{0.02}$ , (c)  $\text{NaLa}_{0.50}(\text{MoO}_4)_2:\text{Ho}_{0.02}/\text{Yb}_{0.45}/\text{Tm}_{0.03}$ , and (d)  $\text{NaLa}_{0.45}(\text{MoO}_4)_2:\text{Ho}_{0.01}/\text{Yb}_{0.50}/\text{Tm}_{0.04}$  particles

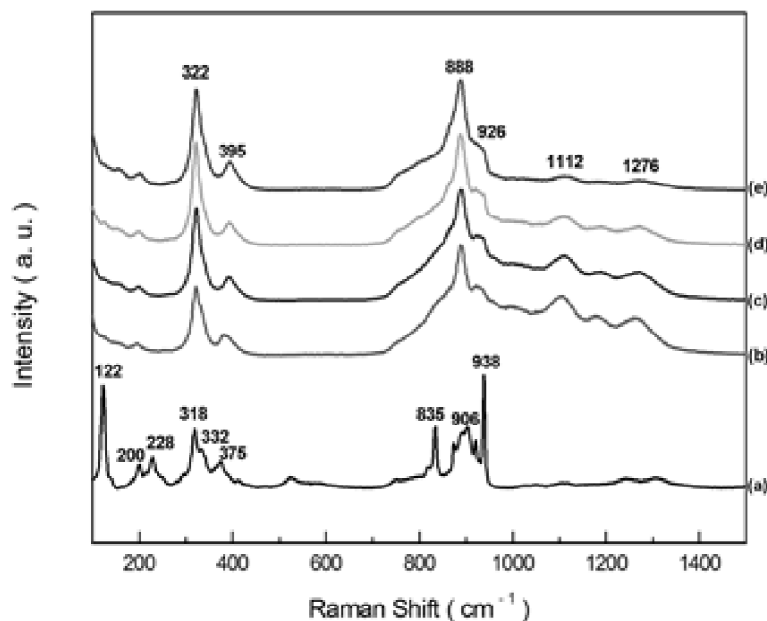


**Figure 6:** Raman spectra of the synthesized (a) pure  $\text{NaLa}(\text{MoO}_4)_2$ , (b)  $\text{NaLa}_{0.60}(\text{MoO}_4)_2:\text{Ho}_{0.04}/\text{Yb}_{0.35}/\text{Tm}_{0.01}$ , (c)  $\text{NaLa}_{0.55}(\text{MoO}_4)_2:\text{Ho}_{0.03}/\text{Yb}_{0.40}/\text{Tm}_{0.02}$ , (d)  $\text{NaLa}_{0.50}(\text{MoO}_4)_2:\text{Ho}_{0.02}/\text{Yb}_{0.45}/\text{Tm}_{0.03}$ , and (e)  $\text{NaLa}_{0.45}(\text{MoO}_4)_2:\text{Ho}_{0.01}/\text{Yb}_{0.50}/\text{Tm}_{0.04}$  particles excited by the 514.5-nm line of an Ar ion laser at 0.5 mW.

shows the chromaticity points for the samples (a), (b), (c), and (d). The chromaticity coordinates ( $x$ ,  $y$ ) are strongly dependent on the  $\text{Ho}^{3+}/\text{Yb}^{3+}/\text{Tm}^{3+}$  concentration ratio. As shown in Fig. 6(A), the calculated chromaticity coordinates  $x = 0.348$  and  $y = 0.350$  for (a),  $x = 0.337$  and  $y = 0.336$  for (b),  $x = 0.335$  and  $y = 0.334$  for (c), and  $x = 0.333$  and  $y = 0.332$  for (d), corresponding to the standard equal-energy point in the CIE diagram in Fig. 6(B).

Fig. 6 shows the Raman spectra of the synthesized (a) pure  $\text{NaLa}(\text{MoO}_4)_2$ , (b)  $\text{NaLa}_{0.60}(\text{MoO}_4)_2: \text{Ho}_{0.04}/\text{Yb}_{0.35}/\text{Tm}_{0.01}$ , (c)  $\text{NaLa}_{0.55}(\text{MoO}_4)_2: \text{Ho}_{0.03}/\text{Yb}_{0.40}/\text{Tm}_{0.02}$ , (d)  $\text{NaLa}_{0.50}(\text{MoO}_4)_2: \text{Ho}_{0.02}/\text{Yb}_{0.45}/\text{Tm}_{0.03}$ , and (e)  $\text{NaLa}_{0.45}(\text{MoO}_4)_2: \text{Ho}_{0.01}/\text{Yb}_{0.50}/\text{Tm}_{0.04}$  particles excited by the 514.5-nm line of an Ar ion laser at 0.5 mW. The internal modes for the (a) pure  $\text{NaLa}(\text{MoO}_4)_2$  particles were detected at 112, 200, 228, 318, 332 and 375  $\text{cm}^{-1}$  on low frequencies, and 835, 906 and 938 on high frequencies. The well-resolved sharp peaks for the  $\text{NaLa}(\text{MoO}_4)_2$  indicate a high crystallinity state of the synthesized particles. The internal vibration-mode frequencies depend on the lattice parameters and the strength of the partially covalent bond between the cation and molecular ionic group  $\text{MO}_4$ . The Raman spectrum of the  $\text{NaLa}(\text{MoO}_4)_2$  crystal in Fig. 6(a) shows the typical molybdate compounds, which are divided into two parts with a wide empty gap of 400~800  $\text{cm}^{-1}$  [30-33]. The stretching vibrations of Mo-O bonds are observed at 835-938  $\text{cm}^{-1}$ . For these stretching vibrations, strong mixing occurs between the Mo-O bonds and the  $\text{MoO}_4$ . The bands at 318 and 375  $\text{cm}^{-1}$  could be assumed to originate from vibrations of the longer Mo-O bonds, which are employed in the formation of the Mo-Mo bridges. The translational vibration motion of the  $\text{Na}^{3+}$  ions is observed around 200~300  $\text{cm}^{-1}$ , whereas the  $\text{La}^{3+}$  translations were located below 180  $\text{cm}^{-1}$  [32, 33]. The Raman spectra of the doped particles (b)-(e) indicate the very strong and dominant peaks at higher frequencies of 888, 926, 1112, and 1276  $\text{cm}^{-1}$  and at lower frequencies of 322 and 395  $\text{cm}^{-1}$ . These strong disordered peaks at higher and lower frequencies are attributed to the superimpositions and the concentration-quenching effect of the  $\text{Ho}^{3+}$  and  $\text{Tm}^{3+}$  ions [34, 35]. These results lead to high emitting efficiency and superior thermal and chemical stability, and these materials can be considered potentially active components in white LED applications.

## Conclusions

White phosphors of  $\text{NaLa}_{1-x}(\text{MoO}_4)_2$  doped with  $\text{Yb}^{3+}$  for a sensitizer and  $\text{Ho}^{3+}/\text{Tm}^{3+}$  for activators were successfully fabricated via MSG process. The resultant particles after annealing at 800°C for 16 h provided well-crystallized and fine morphologies with 3-5  $\mu\text{m}$  of particle sizes. Under excitation derived from 980 nm, the final particles led to the formation of white emissions composed of the red, green, and blue emission features, which are resulted from the transitions of  $\text{Tm}^{3+}$  from the  $^1\text{G}_4 \rightarrow ^3\text{H}_6$  in the blue emission area, the transitions of  $\text{Ho}^{3+}$  from the  $^5\text{S}_2/ ^5\text{F}_4 \rightarrow ^5\text{I}_8$  in the green emission area, as well as the transitions of  $\text{Ho}^{3+}$  from the  $^5\text{F}_5 \rightarrow ^5\text{I}_8$  and the transitions of  $\text{Tm}^{3+}$  from the  $^1\text{G}_4 \rightarrow ^3\text{F}_4$  and  $^3\text{H}_4 \rightarrow ^3\text{H}_6$  in the red emission area. The calculations of the slope value indicated  $n = 1.59$  for green emission at 475 nm,  $n = 1.68$  for green emission at 545 nm, and  $n = 1.85$  and 1.78 for red emissions at 655 and 695 nm, respectively. These strong disordered Raman spectroscopic frequencies were attributed to the superimpositions and the effect of concentration-quenching for the activators for  $\text{Ho}^{3+}$  and  $\text{Tm}^{3+}$  ions.



### Acknowledgment

This research was supported by the Basic Science Research Program through the National Research Foundation of Korea (NRF) funded by the Ministry of Science, ICT and future Planning (2018R1D1A1A09082321).

### References

- [1] C.S. Lim, A. Aleksandrovsky, M. Molokeev, A. Oreshonkov, V. Atuchin, *Phys. Chem. Chem. Phys.*, **17**, 19278 (2015).
- [2] M. Wang, G. Abbineni, A. Clevenger, C. Mao, S. Xu, *Nanomedicine: Nanotech. Biology, and Medicine*, **7**, 710 (2011).
- [3] C. S. Lim, A. Aleksandrovsky, M. Molokeev, A. Oreshonkov, D. Ikonnikov, V. Atuchin, *Dalton Transactions*, **45**, 15541 (2016).
- [4] L. Li, W. Zi, H. Yu, S. Gan, G. Ji, H. Zou, X. Xu, *J. Lumin.*, **143**, 14 (2013).
- [5] C. Ming, F. Song, L. Yan, *Opt. Comm.*, **286**, 217 (2013).
- [6] C.S. Lim, A. Aleksandrovsky, M. Molokeev, A. Oreshonkov, V. Atuchin, *J. Solid State Chemistry*, **228**, 160 (2015).
- [7] J. Jin, K. Yang, J. Su, Z. Si, *J. Lumin.*, **159**, 178 (2015).
- [8] Y. Xu, Y. Wang, L. Xing, X. Tan, *Optics & Laser Tech.*, **54**, 50 (2013).
- [9] D. Li, Y. Wang, X. Zhang, G. Shi, G. Liu, Y. Song, *J. Alloys Compd.*, **550**, 509 (2013).
- [10] J. Tang, C. Cheng, Y. Chen, Y. Huang, *J. Alloys Compd.*, **609**, 68 (2014).
- [11] W. Zhang, J. Li, Y. Wang, J. Long, K. Qiu, *J. Alloys Compd.*, **635**, 16 (2015).
- [12] F. Mo, L. Zhou, Q. Pang, F. Gong, Z. Liang, *Ceram. Inter.*, **38**, 6289 (2012).
- [13] G. Li, S. Lan, L. Li, M. Li, W. Bao, H. Zou, X. Xu, S. Gan, *J. Alloys Compd.*, **513**, 145 (2012).
- [14] J. Liao, H. Huang, H. You, X. Qiu, Y. Li, B. Qui, H-R Wen, *Mater. Res. Bull.*, **45**, 1145 (2010).
- [15] F. Cao, L. Li, Y. Tian, X. Wu, *Optics Laser Tech.*, **55**, 6 (2014).
- [16] G.M. Kuz'micheva, D.A. Lis, K.A. Subbotin, V.B. Rybakov, E.V. Zharikov, *J. Crys. Growth*, **275**, e1835 (2005).
- [17] X. Lu, Z. You, J. Li, Z. Zhu, G. Jia, B. Wu, C. Tu, *J. Alloys Compd.*, **458**, 462 (2008).
- [18] X. Li, Z. Lin, L. Zhang, G. Wang, *J. Crys. Growth*, **290**, 670 (2006).
- [19] Y. K. Voron'ko, K.A. Subbotin, V.E. Shukshin, D.A. Lis, S.N. Ushakov, A.V. Popov, E.V. Zharikov, *Opt. Mater.*, **29**, 246 (2009).
- [20] H. Lin, X. Yan, X. Wang, *J. Sol. State. Chem.*, **204**, 266 (2013).
- [21] G. Li, L. Li, M. Li, W. Bao, Y. Song, S. Gan, H. Zou, X. Xu, *J. Alloys Compd.*, **550**, 1 (2013).
- [22] Y. Huang, L. Zhou, L. Yang, Z. Tang, *Opt. Mater.*, **33**, 777 (2011).
- [23] L. Li, W. Zi, G. Li, S. Lan, G. Ji, S. Gan, H. Zou, X. Xu, *J. Sol. State Chem.*, **191**, 175 (2012).
- [24] Y. Tian, B. Chen, B. Tian, J. Sun, X. Li, J. Zhang, L. Cheng, H. Zhong, Q. Meng, R. Hua, *Physica B.*, **407**, 2556 (2012).
- [25] J. Zhang, X. Wang, X. Zhang, X. Zhao, X. Liu, L. Peng, *Inorg. Chem. Commun.*, **14**, 1723 (2011).
- [26] S.W. Park, B.K. Moon, B.C. Choi, J.H. Jeong, J.S. Bae, K.H. Kim, *Curr. Appl. Phys.*, **12**, S150 (2012).
- [27] C.S. Lim, *Mater. Res. Bull.*, **47**, 4225 (2012).
- [28] R. D. Shannon, *Acta Cryst.*, **A32**, 751 (1976).
- [29] H. Guo, N. Dong, M. Yin, W. Zhang, L. Lou, S. Xia, *J. Phys. Chem. B*, **108**, 19205 (2004).

- [30] V.V. Atuchin, V.G. Grossman, S.V. Adichtchev, N.V. Surovtsev, T.A. Gavrilova, B.G. Bazarov, *Opt. Mater.*, 34, 812 (2012).
- [31] A.A. Savina, V.V. Atuchin, S.F. Solodovnikov, Z.A. Solodovnikova, A.S. Krylov, E.A. Maximovskiy, M.S. Molokeev, A.S. Oreshonkov, A.M. Pugachev, E.G. Khaikina, *J. Solid State Chem.*, 225, 53 (2015).
- [32] V.V. Atuchin, O.D. Chimitova, T.A. Gavrilova, M.S. Molokeev, Sung-Jin Kim, N.V. Surovtsev, B.G. Bazarov, *J. Crys. Growth*, 318, 683 (2011).
- [33] V.V. Atuchin, O.D. Chimitova, S.V. Adichtchev, J.G. bazarov, T.A. Gavrilova, M.S. Molokeev, N.V. Surovtsev, Zh.G. Bazarova, *Mater. Lett.*, 106, 26 (2013).
- [34] C. S. Lim, A, Aleksandrovsky, M. Molokeev, A. Oreshonkov, V. Atuchin, *J. Alloys Compds.*, 695, 737 (2017).
- [35] C. S. Lim, A, Aleksandrovsky, M. Molokeev, A. Oreshonkov, V. Atuchin, *Mater. Lett.*, 181, 38 (2016).